JOURNAL OF GEOPHYSICAL RESEARCH, VOL. 98, NO. D2, PAGES 2729–2739, FEBRUARY 20, 1993

Optical Properties of Marine Stratocumulus Clouds Modified by Ships

MICHAEL D. KING

Laboratory for Atmospheres, NASA Goddard Space Flight Center, Greenbelt, Maryland

LAWRENCE F. RADKE[1] AND PETER V. HOBBS

Department of Atmospheric Sciences, University of Washington, Seattle

The angular distribution of scattered radiation deep within a cloud layer was measured in marine stratocumulus clouds modified by the emissions from ships. These observations, obtained at 13 discrete wavelengths between 0.5 and 2.3 μm, were acquired as the University of Washington C-131A aircraft flew through a pair of roughly parallel ship track signatures produced in clouds off the coast of southern California on July 10, 1987. In the first of these ship tracks, the nadir (upwelling) intensity increased from 40 to 110 W m^{-2} μm^{-1} sr^{-1} at 0.744 μm. The second ship track produced a less dramatic, but more uniform, increase in the upwelling intensity. In contrast, the nadir intensity at 2.20 μm decreased from 1 to 0.13 W m^{-2} μm^{-1} sr^{-1} in the first ship track and to 0.6 W m^{-2} μm^{-1} sr^{-1} in the second ship track. The relative angular distribution of the intensity field at each wavelength was used to determine the similarity parameter, and hence single scattering albedo, of the cloud using the diffusion domain method. Besides the spectral similarity parameter, these measurements provide a good estimate of the optical depth of the cloud layer both above and below the aircraft. Results of this analysis are presented for a 120-km section of marine stratocumulus cloud including both ship tracks. This analysis shows that the total optical thickness of the cloud layer increased in the ship tracks, in contrast to the similarity parameter which decreased. The decrease in absorption was a direct consequence of the reduction in cloud droplet size that occurred within the ship tracks.

> The conclusions which may be drawn from these experiments are—(1) that when water vapour condenses in the atmosphere, it always does so on some solid nucleus; (2) that the dust particles in the air form the nuclei on which it condenses; (3) if there was no dust in the air there would be no fogs, no clouds, no mists, and probably no rain.
>
> J. Aitken (1880)

1. INTRODUCTION

The concentrations of cloud droplets in stratiform clouds are thought to be primarily a function of the concentrations of cloud condensation nuclei (CCN) at a few tenths of 1% supersaturation [*Twomey*, 1959; *Twomey and Warner*, 1967]. The effect of natural and anthropogenic aerosol on cloud structure, cloud chemistry, and solar radiation is an active area of research [e.g., *Twomey*, 1980; *Hudson*, 1983; *Radke*, 1989]. In the remote marine environment, dimethylsulfide produced by phytoplankton is believed to be the major source of CCN after oxidation to form sulfate aerosol [*Bigg et al.*, 1984; *Ayers et al.*, 1991; *Hegg et al.*, 1991]. Anthropogenic sources of pollution can also affect CCN concentrations and cloud droplet size distributions as shown downwind of cane fires in Australia [*Warner and Twomey*, 1967], paper mills in the Pacific Northwest [*Hobbs et al.*, 1970], urban cities such as Denver and St. Louis [*Squires*, 1966; *Braham*, 1974], and the eastern seaboard of the United States [*Radke and Hobbs*, 1976]. Increases in anthropogenic sources of CCN over continents are expected to increase cloud albedo by increasing the concentration and reducing the size of water droplets in low-level water clouds [*Twomey et al.*, 1984]. *Wigley* [1989] has argued that the large increase in SO_2 emissions that has occurred in the northern hemisphere this century may have resulted in enhanced concentrations of sulfate particles and hence CCN, thereby increasing cloud droplet concentrations and in that way producing clouds with higher albedos in the northern hemisphere than in the southern hemisphere. This suggestion is consistent with *Durkee*'s [1990] analysis of 3 years of AVHRR satellite observations over the Pacific Ocean, which shows that the aerosol optical thickness and cloud reflectance at 3.7 μm are both approximately twice as large in the northern hemisphere as in the southern hemisphere.

A striking example of the effects of anthropogenic CCN on cloud radiative properties can be found in satellite observations of marine stratocumulus clouds modified by emissions from ships. These so-called "ship tracks" in clouds were first observed in satellite imagery under conditions in which exhaust particles emitted by ships were responsible for producing a visible cloud in otherwise cloud-free conditions as deduced by satellite [*Conover*, 1966]. *Coakley et al.* [1987] and *Albrecht* [1989] further noted the frequent and long-lived occurrence of ship track signatures in preexisting stratus and stratocumulus clouds, as evident by the enhanced reflectance of the clouds produced by exhaust from these ships, especially at 3.7 μm [see *Scorer*, 1987]. During the marine stratocumulus intensive field observation (IFO) component of the First ISCCP Regional Experiment (FIRE), conducted off the coast of southern California during July 1987 [*Albrecht et al.*, 1988], we obtained the first in situ microphysics and solar radiation measurements of clouds modified by pollution from ships. Selected radiative and microphysical properties of these clouds, together with AVHRR satellite images, were previously described by *Radke et al.* [1989].

[1]Now at National Center for Atmospheric Research, Boulder, Colorado.

Paper number 92JD02082.
0148-0227/93/92JD-02082$05.00

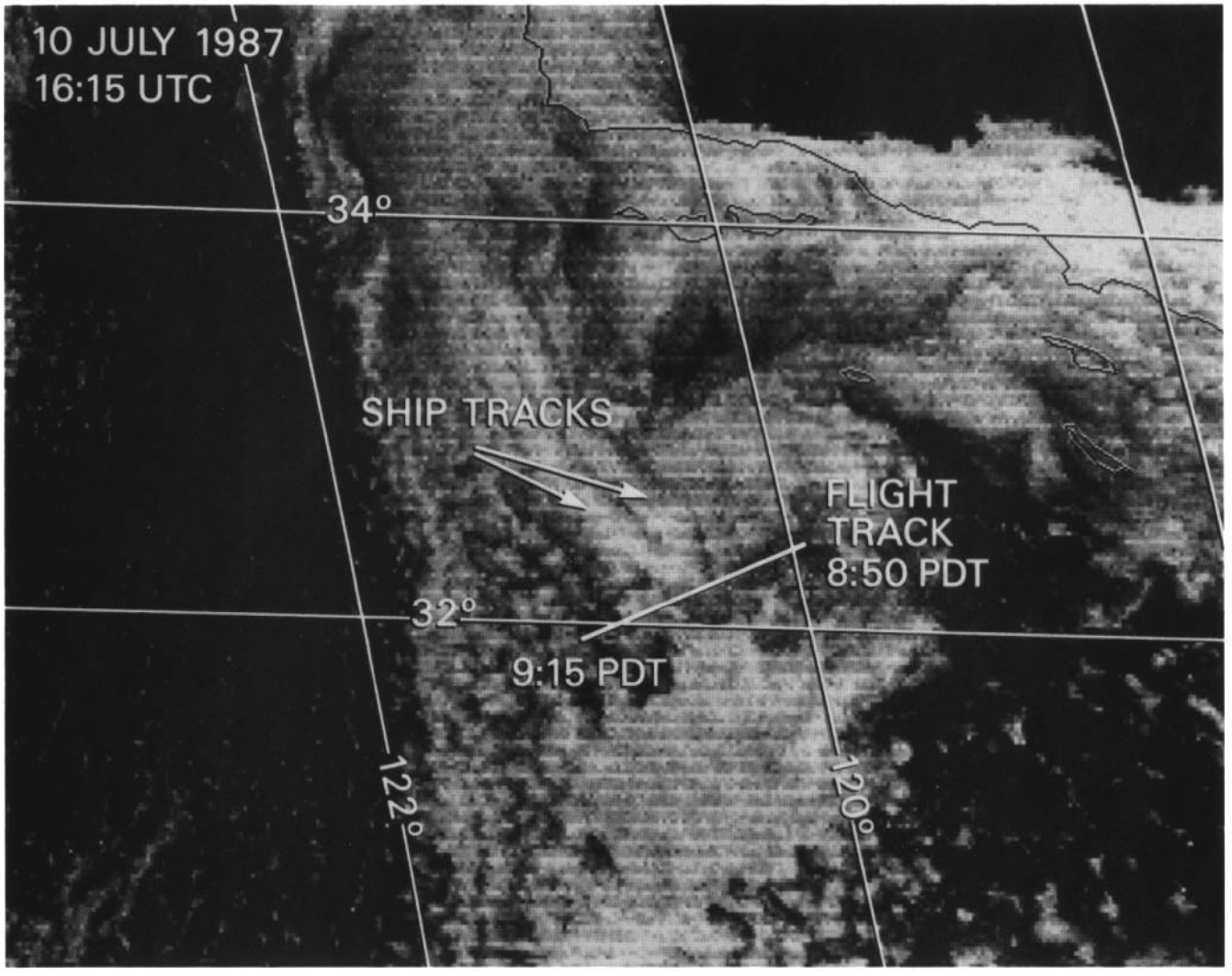

Fig. 1. GOES 6 visible image for 1615 UTC (0915 PDT) on July 10, 1987. The image encompasses the FIRE marine stratocumulus region and includes the flight track of the C-131A aircraft between 0850 and 0915 PDT. The arrows indicate the pair of roughly parallel ship tracks penetrated by the aircraft.

In this paper, we present internal scattered radiation measurements at selected wavelengths between 0.5 and 2.3 μm that were obtained in the same 120-km section of marine stratocumulus clouds containing these two ship track features. The angular distribution of scattered radiation in a vertical plane on the right-hand side of the aircraft was measured aboard the University of Washington's Convair C-131A research aircraft using the cloud absorption radiometer (CAR) described by *King et al.* [1986]. In addition to the radiation measurements, the cloud microphysical structure, including cloud droplet size distribution and liquid water content, were monitored continuously with instruments aboard the aircraft. Finally, we present the optical thickness and spectral absorption of the cloud layer derived from scattered solar radiation measurements using the diffusion domain method [*King*, 1981; *King et al.*, 1990].

2. Summary of Observations

Measurements of the radiative and microphysical properties of clouds modified by the emissions from ships were obtained off the coast of southern California on July 10, 1987, as part of the FIRE IFO program [*Radke et al.*, 1989]. On this day the C-131A aircraft was flying within a marine stratocumulus cloud layer about 400 m thick enroute to a coordinated mission with the NASA ER-2 aircraft when it encountered two anomalous regions of cloud, each approximately 10–15 km in width, that exhibited substantial differences in cloud radiative and microphysical properties from the surrounding cloud. Figure 1 illustrates a GOES 6 visible image of marine stratocumulus cloud obtained at 1615 UTC (0915 PDT) on July 10. Superimposed on this figure is the location of the C-131A flight track between 0850 and 0915 PDT. As is common for marine stratocumulus clouds of the eastern Pacific, these clouds were under the influence of a high-pressure system centered near 35°N, 140°W, which produced a cloud pattern aligned with the boundary layer winds from the north. The bright lines of clouds between 33.5°N, 121.0°W and 32.5°N, 120.5°W are the two anomalous cloud regions referred to above, which were penetrated by the aircraft at 0857–0859 and 0905–0908 PDT. A corresponding image obtained with the NOAA 10 AVHRR at 0838 PDT can be found in the work by *Radke et al.* [1989]. We attribute

these two anomalous regions of cloud to ship tracks, as described below.

3. CLOUD MICROPHYSICAL MEASUREMENTS

The University of Washington C-131A research aircraft is well equipped for measuring cloud microphysical properties. The primary instruments of interest to the present investigation of water clouds are: (1) a Johnson-Williams hot wire probe for measuring the cloud liquid water content, and (2) three Particle Measuring Systems Inc. (PMS) probes for measuring the cloud droplet size distribution. These size distribution measurements were obtained using an FSSP-100, an OAP-200X cloud probe, and an OAP-200Y precipitation probe to cover the radius range from 1.4 to 2250 μm. Detailed descriptions of these instruments can be found in the work by *Knollenberg* [1981].

Plate 1 depicts the cloud droplet size distribution as a function of distance along the flight track for measurements obtained within the stratocumulus cloud layer between 0850 and 0915 PDT on July 10, 1987. At the average ground speed of 80 m s^{-1}, this image corresponds to a flight distance of 120 km. The aircraft was flying at an altitude of 725 m near the middle of the cloud layer, which was itself about 440 m thick as determined by profile descent measurements obtained through a stratocumulus cloud layer some 130 km south and 1 hour 50 min later than the ship track penetration. The measurements presented in Plate 1 were acquired with the FSSP-100 and OAP-200X, and extend the corresponding FSSP-only image that was presented by *Radke et al.* [1989]. The concentrations of droplets measured with the OAP-200Y ($r \geq 150$ μm) were generally too small to be significant and are therefore omitted from Plate 1.

The ship track features centered near 38 and 78 km are readily apparent in Plate 1 as having an enhanced concentration of small droplets, a reduced mode radius, a reduced concentration of drizzle-sized droplets ($r \gtrsim 100$ μm), and a narrower cloud droplet size distribution. This reduction in the concentration of drizzle-sized droplets, first suggested by *Albrecht* [1989] and observed by *Radke et al.* [1989], can also be seen in Figure 2, which contrasts the cloud droplet size distribution in portions of the cloud affected by ships with corresponding portions of the cloud "uncontaminated" by ship track effluents. These results represent averages of measurements obtained using the FSSP-100 (squares) and OAP-200X cloud probe (circles), where the solid symbols correspond to the portions of the cloud affected by ships and the open symbols to uncontaminated cloud. The droplet size distribution of the uncontaminated cloud has a larger concentration of drizzle droplets than does the cloud affected by ships, a characteristic that was frequently observed during the FIRE marine stratocumulus IFO [*Albrecht*, 1989; *Radke et al.*, 1989].

From measurements of the cloud droplet size distribution it is straightforward to calculate both the total concentration and effective radius of the cloud droplets, where the effective radius r_e is defined by [*Hansen and Travis*, 1974]:

$$r_e = \int_0^\infty r^3 n(r)\, dr \Big/ \int_0^\infty r^2 n(r)\, dr, \qquad (1)$$

where $n(r)$ is the concentration of cloud droplets in the radius range r to $r + dr$. Figures 3 and 4 show the droplet concentration and effective radius as a function of distance (or time) for measurements obtained inside clouds between 0850 and 0915 PDT. These results, obtained from the size distribution measurements presented in Plate 1, clearly show the dramatic increase in droplet concentration and decrease in effective radius in both regions of cloud affected by ships. These are just the effects to be expected from clouds modified by effluents from ships in otherwise pristine marine air. Figure 5 shows a corresponding time series of cloud liquid water content measured with the Johnson-Williams hot wire probe, and demonstrates that the liquid water content is substantially enhanced in both ship track regions, as reported by *Radke et al.* [1989].

The increased droplet concentration, decreased particle size, and increased liquid water content that we observed in both ship track features that we penetrated on July 10 all act in such a way as to increase the optical thickness of the portions of the cloud affected by ships. This is consistent with the increased reflectance of the clouds along the ship tracks that we reported from AVHRR satellite imagery [*Radke et al.*, 1989], and which is apparent in the GOES 6 visible image presented in Figure 1.

4. RADIATION MEASUREMENTS

In addition to cloud microphysical properties, the C-131A aircraft carries a cloud absorption radiometer (CAR) developed at Goddard Space Flight Center. This instrument, a 13-channel scanning radiometer mounted in the nose of the aircraft, scans in a vertical plane from 5° before zenith to 5° past nadir (190° aperture) with an instantaneous field of view of 1°. This permits observations of the angular distribution of scattered radiation from zenith to nadir at 13 discrete wavelengths between 0.5 and 2.3 μm with as much as a 5° roll of the aircraft. A detailed description of this instrument can be found in the work of *King et al.* [1986].

Figures 6 and 7 illustrate the zenith and nadir intensities as a function of distance (time) for measurements obtained inside clouds for a 120-km section of the cloud studied on July 10, 1987. These data, corresponding to observations obtained with the cloud absorption radiometer at 0.744 and 2.20 μm, respectively, show that the zenith and nadir intensities were substantially modified by the ships. At $\lambda = 0.744$ μm (Figure 6), for example, the upwelling (nadir) intensity increased from approximately 40 to 110 W m^{-2} μm^{-1} sr^{-1} in the first ship track, with a somewhat less dramatic, though more uniform, increase in the second ship track. The downwelling (zenith) intensity, on the other hand, showed a modest decrease in both ship tracks. These changes are consistent with the fact that the total optical thickness of the cloud layer increased, and are a direct consequence of the observation that the total concentration and concentration of small droplets increased, while the mean droplet radius decreased.

At $\lambda = 2.20$ μm (Figure 7), both the upwelling (nadir) and downwelling (zenith) intensities decreased within the ship tracks. Again, the change is the most dramatic and the least uniform in the first ship track. The explanation for these changes can be understood as follows. As the optical thickness increases, the additional scattering leads to increased attenuation of solar radiation at this absorbing wavelength. The intensity distribution is thus reduced in all directions within the cloud. This is not the case for reflected solar

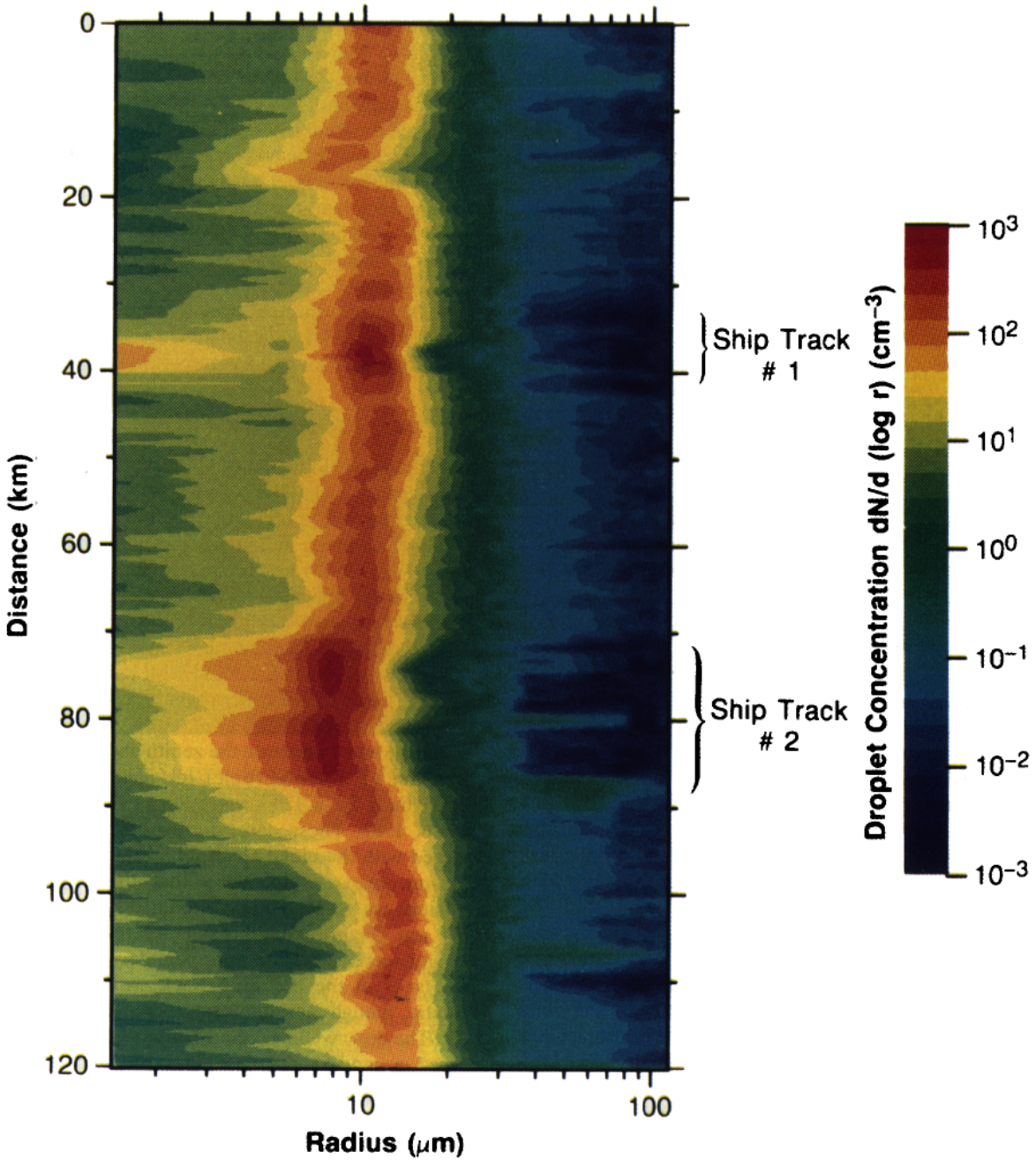

Plate 1. False color image of the cloud droplet size distribution as a function of distance along the flight path for a 120-km section of marine stratocumulus clouds on July 10, 1987. In both ship track features there is an enhanced concentration of small droplets and a significant reduction of drizzle-sized droplets ($r \approx 100$-μm radius).

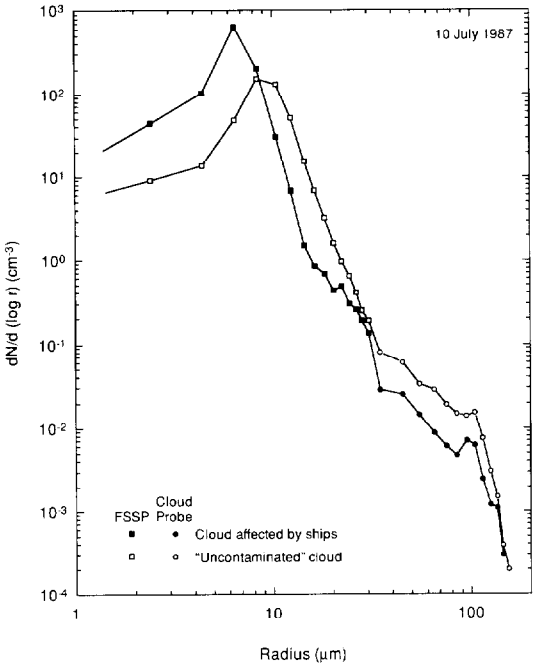

Fig. 2. The average cloud drop size distribution in marine stratocumulus cloud affected by ships and in uncontaminated portions of the cloud on July 10, 1987. Note the reduced concentration of drizzle-sized droplets in the ship track-modified cloud layer compared to the uncontaminated portions of the cloud. The data points represent averages of measurements obtained with the PMS FSSP-100 (squares) and PMS OAP-200X cloud probe (circles). The solid symbols represent averages of all size distribution measurements having an effective droplet radius (r_e) in the range $7 \leq r_e \leq 8$ μm, whereas the open symbols pertain to distributions for which $11 \leq r_e \leq 12$ μm.

radiation, since increasing the optical thickness will always lead to an increased reflection function at all wavelengths, provided the scattering layer (cloud) overlies a dark surface such as the Pacific Ocean.

Figures 6 and 7 represent dramatically different single scattering albedos of the cloud layer. At $\lambda = 0.744$ μm the

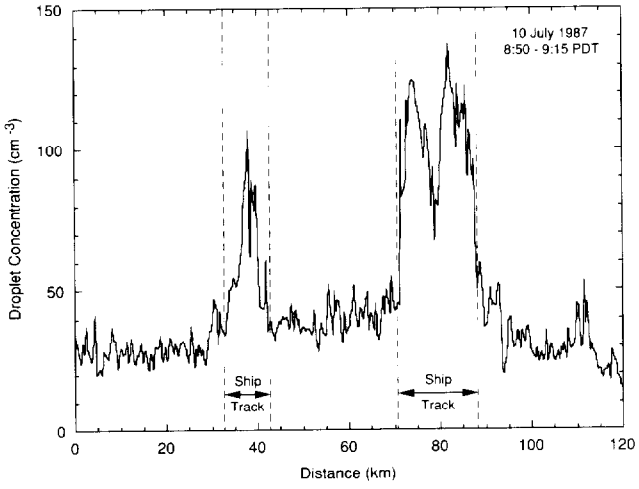

Fig. 3. Cloud droplet concentration as a function of distance along the flight track for measurements obtained inside clouds between 0850 and 0915 PDT on July 10, 1987.

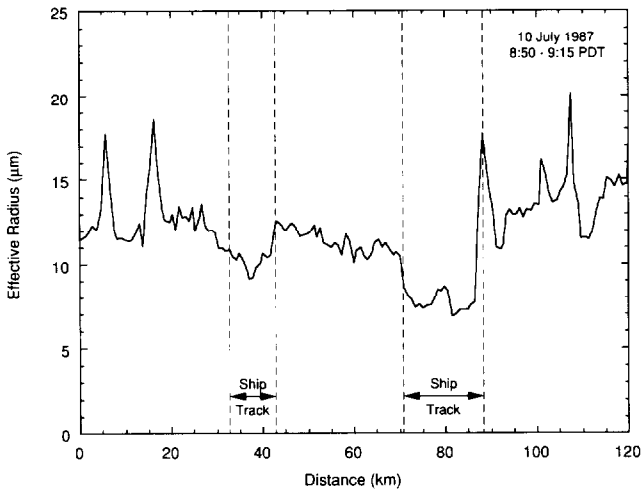

Fig. 4. As in Figure 3 except for the effective radius of the cloud drops.

single scattering albedo $\omega_0 \simeq 1.0$, whereas at $\lambda = 2.20$ μm $\omega_0 \simeq 0.99$ [cf. *King et al.*, 1990]. To examine the transition of the zenith and nadir intensities as the single scattering albedo, and hence wavelength, varies, we have examined the nadir intensity (Figure 8) and zenith intensity (Figure 9) for selected wavelengths between 0.744 and 2.20 μm. The curves for 0.744 and 2.20 μm are the same as those presented in Figures 6 and 7. For the nadir (upwelling) intensity (Figure 8), the transition from an enhanced intensity at 0.744 μm to a reduced intensity at 2.20 μm is quite striking. At some wavelength between 1.20 and 1.64 μm, these results suggest that the changes in the optical properties of the cloud affected by ships would be imperceptible. The broadband pyranometer measurements, which integrate over all angles as well as the entire solar spectrum, follow very closely the changes that we observed with the CAR at 0.744 μm [cf. *Radke et al.*, 1989].

For the zenith (downwelling) intensity, illustrated in Figure 9, the intensity decreases at all wavelengths, though the reduction at 0.744 μm is extremely small, as noted previously in Figure 6. The effect of increasing absorption as the

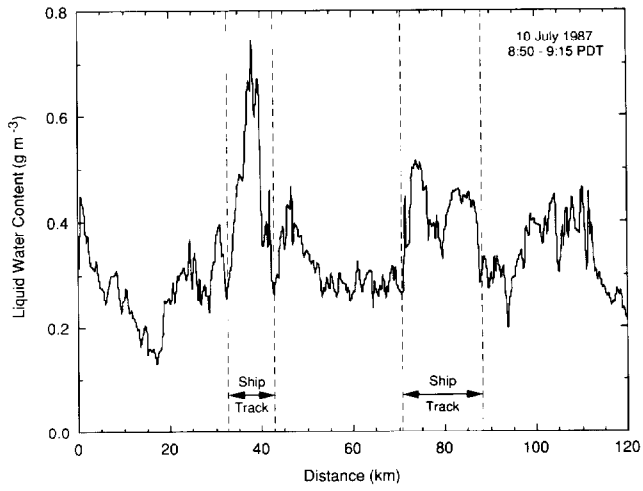

Fig. 5. As in Figure 3 except for the cloud liquid water content.

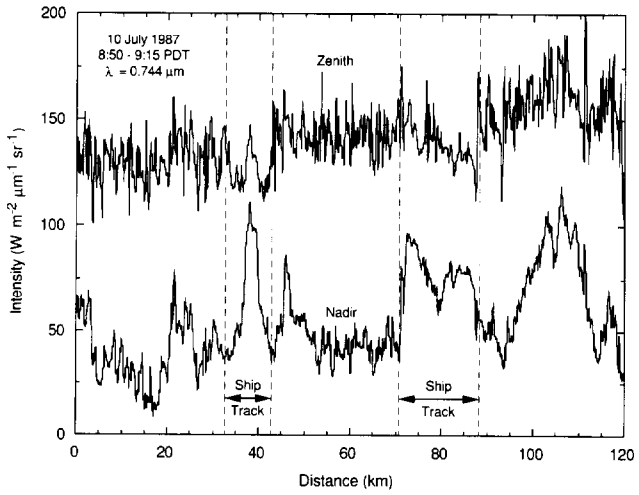

Fig. 6. Zenith and nadir intensities as a function of distance along the flight track for measurements obtained inside clouds between 0850 and 0915 PDT. These measurements were obtained at a wavelength of 0.744 μm.

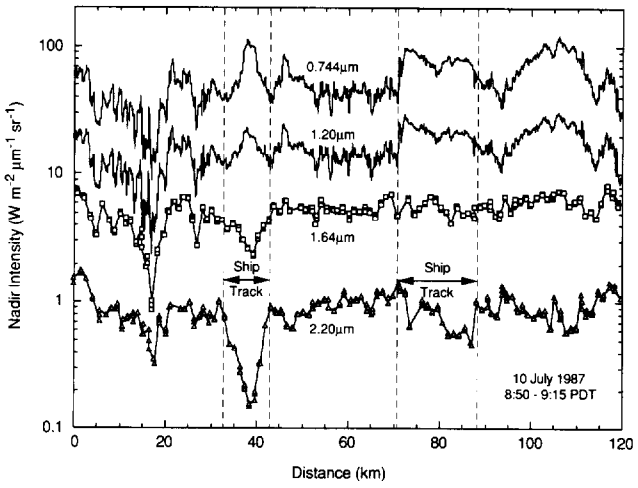

Fig. 8. Nadir (upwelling) intensities as a function of distance for measurements obtained inside clouds between 0850 and 0915 PDT. These measurements were obtained at selected wavelengths between 0.744 and 2.20 μm.

wavelength increases is readily apparent in this figure as an increasingly large decrease in the transmitted intensity field, especially evident in the ship track features. The broadband pyranometer, which again reflects primarily the measurement at nonabsorbing wavelengths near 0.744 μm, shows that the downwelling flux was reduced slightly in the ship tracks, as anticipated from an examination of Figure 9.

5. Results From Observations

Although the major changes in the internal scattered radiation field within the ship track-modified marine stratocumulus clouds can be explained by changes in cloud optical thickness, both above and below the aircraft, it is conceivable that soot particles from the ship exhaust could also have a direct effect on the spectral intensity field within the clouds. In fact, one might argue that, in addition to increasing optical thickness by the emission of cloud condensation nuclei, the ship exhaust could lead to increased absorption by the cloud droplets. Two competing effects are thus possible: (1) increased absorption from aerosols, either as a result of dirty water or interstitial aerosol; and (2) decreased absorption because the cloud droplets are smaller.

To assess the importance of these two effects on the ship track-modified clouds that we observed, we applied the diffusion domain method to the radiation measurements presented in Figures 8 and 9. In this method, described in detail by *King et al.* [1990], the intensity of scattered radiation deep within a cloud layer is measured as a function of zenith angle for selected wavelengths in the visible and near-infrared. To be applicable, therefore, the measurements must be obtained within the diffusion domain of an optically thick medium, defined as a region sufficiently far from the top and bottom boundaries of the cloud such that the diffuse radiation field assumes an asymptotic form characterized by rather simple properties. In particular, the angular intensity distribution becomes azimuthally independent and monotonically decreasing from zenith to nadir, with the relative angular distribution of scattered radiation being

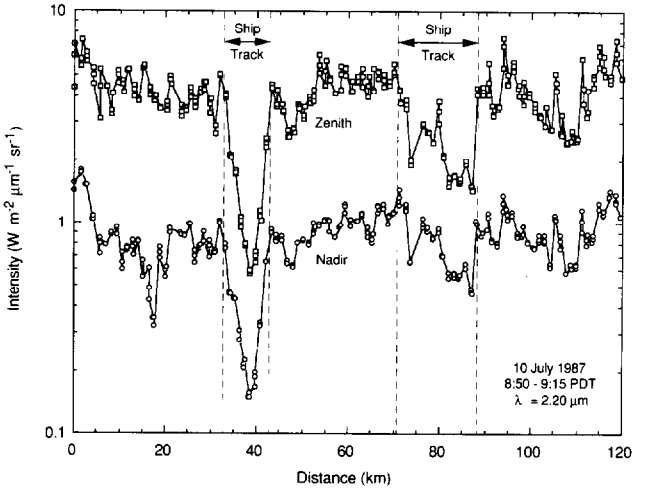

Fig. 7. As in Figure 6 except for a wavelength of 2.20 μm.

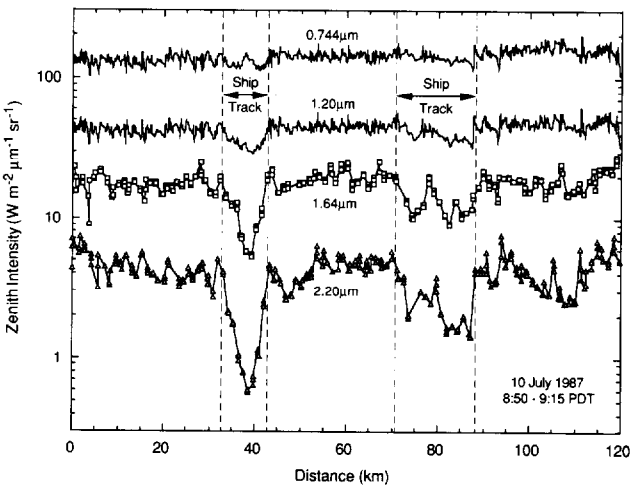

Fig. 9. As in Figure 8 except for zenith (downwelling) intensities.

TABLE 1. Spectral Reflectance of the Pacific Ocean (A_g) on July 10, 1987

Optical Channel	Wavelength, μm	Ocean Reflectance
1	0.503	0.0742 ± 0.0079
2	0.673	0.0606 ± 0.0076
3	0.744	0.0634 ± 0.0078
4	0.866	0.0608 ± 0.0078
5	1.031	0.0555 ± 0.0079
6	1.198	0.0500 ± 0.0082
7	1.247	0.0542 ± 0.0085
8	1.547	0.0432 ± 0.0151
9	1.640	0.0426 ± 0.0086
10	1.722	0.0389 ± 0.0045
11	1.996	0.0148 ± 0.0165*
12	2.200	0.0174 ± 0.0120*
13	2.289	0.0215 ± 0.0097*

*Adjusted to compensate for saturation of the transmitted intensity field in directions near the zenith.

independent of the solar zenith angle and a strong function of the similarity parameter s, defined by

$$s = \left(\frac{1 - \omega_0}{1 - \omega_0 g}\right)^{1/2}, \qquad (2)$$

where g is the asymmetry factor and ω_0 the single scattering albedo of a small volume of cloud air.

Using asymptotic theory for thick layers, *King* [1981] showed that the ratio of the nadir-to-zenith intensities within the diffusion domain of an optically thick medium is solely a function of the surface reflectance (A_g), similarity parameter (s), and scaled optical depth between the aircraft flight level and the base of the cloud [$(1 - g)(\tau_c - \tau)$]. Since the measurements presented in Figures 6–9 were acquired over the Pacific Ocean some 300 km west of San Diego, the spectral reflectance of the ocean surface was small, quite uniform, and easy to characterize. We determined A_g for each channel of the CAR by assuming the transmitted intensity field beneath optically thick clouds is azimuthally independent, thereby permitting us to integrate our transmitted intensity measurements over zenith angle to obtain estimates of the spectral fluxes in the upward and downward hemispheres. Table 1 summarizes the spectral surface reflectances and corresponding standard deviations obtained from this analysis for all 13 channels of the CAR. Slight adjustments have been made for channels 11–13, since the transmitted intensity field experienced some saturation in the zenith direction in each of these channels.

To determine which measurements in Figures 6–9 are within the diffusion domain, we developed a comprehensive set of tests to which the CAR data were subjected. These tests, described in detail by *King et al.* [1990], are based on the fact that the angular intensity field in the diffusion domain of an optically thick, conservatively scattering medium varies as the cosine of the zenith angle (namely, $I(\tau, \cos\theta) = a + b \cos\theta$). We have applied these criteria to channel 1 ($\lambda = 0.503$ μm) of the CAR for each of the 2363 scans presented in Figures 8 and 9, from which we conclude that 586 scans met these criteria.

Once the portions of a flight containing diffusion domain measurements have been identified, it is rather straightforward to analyze the measurements to derive the spectral similarity parameter of the clouds using the diffusion domain method. Before applying this method to the experimental observations presented in Figures 8 and 9, it was first necessary to calculate the relative optical thickness and asymmetry factor of water clouds as a function of wavelength for the cloud layer having the measured cloud droplet size distribution. Due to the large variability in cloud microphysical properties for this section of cloud, we found it necessary to subdivide the data into subsections for which the effective radius was relatively constant. We therefore chose to perform these single scattering calculations for 14 different size distributions, each of which represented an average of all measured size distributions within an effective radius range of 1 μm (e.g., $7 \le r_e < 8$ μm). Figure 2 illustrates two of these size distributions, one having an effective radius in the range $7 \le r_e < 8$ μm, characteristic of ship track contaminated clouds, and the other having r_e in the range $11 \le r_e < 12$ μm, characteristic of uncontaminated clouds. The single scattering computations required a blend of Mie theory for size parameters ($2\pi r/\lambda$) less that 100 and complex angular momentum (CAM) theory [*Nussenzveig and Wiscombe*, 1980] for size parameters greater than 100. The use of CAM theory permitted us to efficiently calculate the spectral optical thickness and asymmetry factor for measured droplet size distributions containing an appreciable number of large drizzle drops, drop sizes that would otherwise be prohibitively expensive to include in Mie theory computations.

The scaled optical depth between the aircraft flight level and the base of the cloud was derived for each scan line of Figure 6 that satisfied the diffusion domain criteria. The lower curve in Figure 10 illustrates the optical depth $\tau_c - \tau$ as a function of distance, where we converted scaled optical depth to optical depth using the asymmetry factor applicable to this wavelength ($\lambda = 0.744$ μm). Of the 586 scan lines that passed our restrictive diffusion domain criteria, the vast majority were in the optically thick regions containing ship track signatures and in the optically thick region between 100 and 110 km that corresponds to the stratocumulus cellular

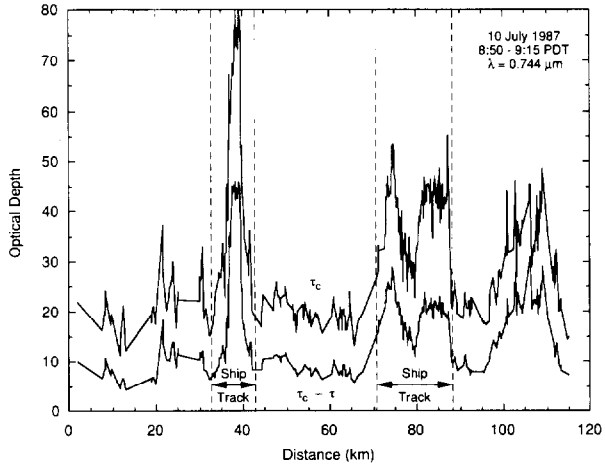

Fig. 10. Optical depth as a function of distance along the flight track for all measurements in Figure 6 that satisfy the diffusion domain criteria. The lower curve represents the optical depth beneath the aircraft ($\tau_c - \tau$) and the upper curve the total optical thickness of the cloud layer (τ_c). All results were derived from measurements at $\lambda = 0.744$ μm.

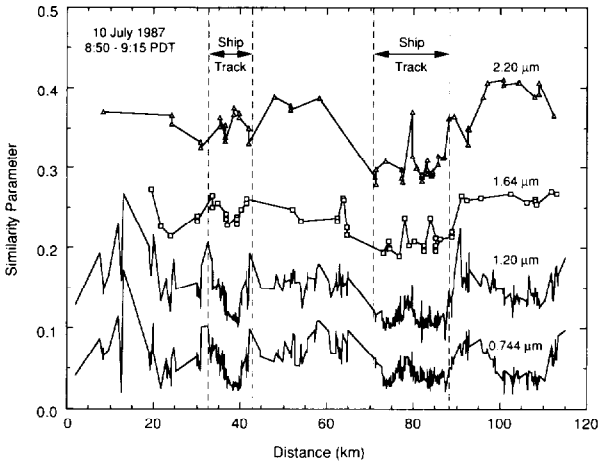

Fig. 11. Similarity parameter as a function of distance for four wavelengths between 0.744 and 2.20 μm.

region clearly evident in the GOES 6 visible image toward the end of the C-131A flight track (cf. Figure 1). As expected, the ship track measurements between 35 and 40 km corresponded to the region of cloud having the largest optical depth beneath the aircraft, since the angular intensity measurements obtained in this region of cloud were the most nearly isotropic of the measurements that we obtained (cf. Figure 6).

Given the surface reflectance and optical depth beneath the aircraft for an individual scan of the radiometer at a specified wavelength, the intensity ratio $I(\tau, -1)/I(\tau, 1)$ is reduced solely to a function of the similarity parameter s. Utilizing this relationship, described in detail by *King et al.* [1990], we were able to calculate the intensity ratio as a function of similarity parameter and match this functional relationship with the measured intensity ratio to derive a value of the similarity parameter for a given measurement and wavelength.

Figure 11 illustrates the similarity parameter as a function of distance for four wavelengths of the CAR. This analysis is based entirely on the ratio of the nadir-to-zenith intensities obtained from the measurements presented in Figures 8 and 9, and as such is entirely independent of the absolute calibration of the radiometer. The decrease in the similarity parameter that we obtain within the ship track-modified cloud layer is a direct consequence of the fact that the effective radius of the cloud droplets decreased (cf. Figure 4), since the similarity parameter s is proportional to $r_e^{1/2}$ [*Twomey and Bohren*, 1980]. These results are in no way due to a decrease in the imaginary part of the complex refractive index of the cloud droplets themselves. Due to the use of a filter wheel to measure the intensity field in channels 8–13, diffusion domain measurements were obtained in this time interval for between 71 and 79 scans, depending on filter position, in contrast to 586 scans for the first seven, simultaneously sampled channels.

Finally, in order to determine the optical depth (τ) above the aircraft, and hence the total optical thickness (τ_c) of the cloud layer, it is necessary to make use of the absolute intensity measurements in a particular direction (say nadir), in combination with the values of $\tau_c - \tau$, A_g and s derived previously from relative intensity measurements. *King et al.* [1990] showed that in the diffusion domain of an optically thick layer, the nadir (upwelling) intensity $I(\tau, -1)$ can be written as

$$I(\tau, -1) = s_1 P(1) e^{-k\tau}\left[D - \left(l - \frac{A_g m n^2}{1 - A_g A^*}\right) e^{-2k(\tau_c - \tau)}\right], \tag{3}$$

where

$$s_1 = \frac{\mu_0 F_0 (1 - A_g A^*) K(\mu_0)}{\pi[(1 - A_g A^*)(1 - l^2 e^{-2k\tau_c}) + A_g m n^2 l e^{-2k\tau_c}]}. \tag{4}$$

In these expressions, k is the diffusion exponent (eigenvalue) describing the vertical attenuation of radiation in the diffusion domain, $P(u)$ the diffusion pattern (eigenfunction), u the cosine of the zenith angle with respect to the positive τ direction ($-1 \le u \le 1$), μ_0 the cosine of the solar zenith angle, F_0 the incident solar flux, $K(\mu_0)$ the escape function, s_1 the strength of the diffusion stream in the positive τ direction, A^* the spherical albedo of a semi-infinite atmosphere, D the diffusion pattern ratio $P(-1)/P(1)$, and m, n, and l constants.

All six asymptotic constants that appear in these expressions [A^*, D, m, n, l, and $k/(1 - g)$] may be accurately represented by a function of the similarity parameter s, as demonstrated by *King* [1981]. Thus, from our analysis of s at 0.744 μm, obtained by applying the diffusion domain method to relative intensity measurements (cf. Figure 11), it is rather straightforward to calculate the asymptotic constants arising in (3) and (4) using the similarity relations given by *King et al.* [1990]. The diffusion pattern $P(1)$ can be estimated by noting that when s is small, as it is for $\lambda = 0.744$ μm, the diffusion pattern $P(u) = a + bu$, the assumption for the angular distribution of scattered radiation in the Eddington approximation. Hence, by combining the definition of $D = P(-1)/P(1)$ with the definition of m, given by

$$m \simeq 2\int_{-1}^{1} [P(u)]^2 u\,du,$$

it can readily be shown that $P(1)$ can be approximated by the expression:

$$P(1) \simeq \left[\frac{3m}{2(1 + D)(1 - D)}\right]^{1/2}, \tag{5}$$

which can readily be evaluated using the similarity relations for m and D.

The solar zenith angle θ_0 decreased from 56.7° at the beginning of the time series (0850 PDT) to 52.6° at the end (0915 PDT). For small absorption the escape function $K(\mu_0)$ can be related to the escape function for conservative scattering $K_0(\mu_0)$, which itself is very nearly a linear function of μ_0 [*van de Hulst*, 1980]. For anisotropic cloud phase functions appropriate to water clouds at visible wavelengths, it is therefore sufficient to approximate $K(\mu_0)$ as follows:

$$K(\mu_0) \simeq (1 - q_0 k)(0.4384 + 0.8529\mu_0), \tag{6}$$

where q_0 is the extrapolation length. It is sufficiently accurate to approximate the reduced extrapolation length $q' = (1 - g)q_0$ by 0.714 [*King*, 1981]. Substituting these expressions and values into (3) and (4), we were thus able to

TABLE 2. Optical and Microphysical Properties of Marine Stratocumulus Clouds Modified by Emissions From Ships

	Ship Track	Uncontaminated Cloud	Ship Track	Ship Track
Distance	38 km	63 km	74 km	82 km
Microphysical properties				
N, cm^{-3}	104	41	125	137
r_e, μm	9.7	10.3	7.6	6.9
W, g m^{-3}	0.72	0.30	0.51	0.46
Optical properties				
τ_c	67.3	20.2	43.6	44.5
$\tau_c - \tau$	44.7	9.1	24.9	22.7
s	0.0335	0.0817	0.0339	0.0344
g	0.8577	0.8589	0.8512	0.8496
ω_0	0.99984	0.99905	0.99983	0.99982

All optical properties apply at $\lambda = 0.744$ μm.

compute τ_c (and hence τ) as a function of flight track distance.

Figure 10 illustrates the total optical thickness (τ_c) as well as the optical depth beneath the aircraft ($\tau_c - \tau$) as a function of flight track distance for all measurements presented in Figure 6 that satisfy the diffusion domain criteria. These results, together with the similarity parameter derived and presented in Figure 11, demonstrate that the radiative properties of marine stratocumulus clouds affected by pollution from ships can be explained as follows: (1) an increase in the total optical thickness of the cloud layer, (2) a reduced effective radius of the cloud droplets, and (3) a reduced similarity parameter (increased single scattering albedo) of the cloud droplets. Table 2 summarizes the optical and microphysical properties of marine stratocumulus clouds derived from our analysis of two ship track signatures observed on July 10, 1987.

6. SUMMARY AND CONCLUSIONS

In this paper we have presented results of an application of the diffusion domain method to multispectral solar radiation measurements obtained deep within a marine stratocumulus cloud layer modified by pollution from ships. In this method, in situ airborne measurements of the relative angular distribution of scattered radiation are compared to known asymptotic expressions for the intensity field deep within an optically thick cloud layer. Analytic expressions relating the ratio of the nadir-to-zenith intensities to surface reflectance (A_g), similarity parameter (s), and scaled optical depth beneath the aircraft flight level [$(1 - g)(\tau_c - \tau)$] were used to analyze measurements obtained with the cloud absorption radiometer [*King et al.*, 1986] mounted in the nose of the University of Washington's C-131A research aircraft.

The measurements presented in this article were acquired in a layer of clean marine stratocumulus cloud approximately 400 m thick and located about 300 km west of San Diego, California. The aircraft was flying at 725 m near the middle of the cloud layer when it encountered two regions of cloud having anomalous microphysical and radiative properties. We attribute these anomalies to regions of influence from ships, as evidenced by the large increase in the cloud droplet concentration, decrease in effective particle radius, and increase in the liquid water content (cf. Figures 3–5). The angular scattering measurements within the cloud layer show that the nadir (upwelling) intensity field increased at a weakly absorbing wavelength (0.744 μm) and decreased in the near-infrared (2.20 μm) where absorption by liquid water is significant, in contrast to nearby clouds unaffected by ships (cf. Figures 6 and 7). Furthermore, the zenith (downwelling) intensity field decreased at all wavelengths but the greatest decrease occurred at wavelengths for which the absorption by cloud water was the greatest.

To apply the diffusion domain method to these experimental observations, it was first necessary to determine whether the observations were made far enough from the top and bottom boundaries of a sufficiently thick cloud to be within the diffusion domain, defined as a region where the diffuse radiation field assumes an asymptotic form characterized by rather simple properties. This has been accomplished by comparing the measured intensity as a function of zenith angle with that expected from theory for a nonabsorbing or weakly absorbing wavelength, as described in detail by *King et al.* [1990]. An application of this method, which consists of multiple criteria for establishing that the measurements were obtained within the diffusion domain, resulted in 586 of the 2363 scans presented in Figures 8 and 9 meeting these criteria. In general, these scans were obtained in the optically thickest (ship track-contaminated) portions of the cloud layer.

Once the angular scans containing diffusion domain measurements have been determined, it is rather straightforward to analyze these measurements to derive the scaled optical depth beneath the aircraft as well as the spectral similarity parameter of the clouds at each of the CAR wavelengths. These results, obtained using the diffusion domain method, are presented in Figures 10 and 11, where the conversion from scaled optical depth to optical depth was based on the asymmetry factor calculated from the measured cloud droplet size distribution appropriate to the section of cloud being analyzed. Finally, the determination of the optical depth above the aircraft, and hence the total optical thickness of the cloud layer, required an application of asymptotic theory to calibrated intensity measurements in the nadir (zenith propagating) direction. In addition to the nadir intensity $I(\tau, -1)$ and solar zenith angle θ_0, this analysis requires a knowledge of the scaled optical depth $(1 - g)(\tau_c - \tau)$, similarity parameter s, and surface reflectance A_g at the wavelength of the measurements (in this case 0.744 μm). This analysis is greatly simplified by knowing the asymptotic form of the scattered intensity field as well as formulas for

the asymptotic constants [*King et al.*, 1990] and functions (equations (5) and (6)) that appear in this formula (equation (3)). The total optical thickness of the cloud layer obtained from such analysis is presented as the upper curve in Figure 10.

Our analysis of the experimental observations presented in Figures 6–9 shows that the total optical thickness of the cloud layer increased from 20 to 67 in the first ship track and to 44 in the second ship track. In contrast, the single scattering albedo at 0.744 μm increased from 0.99905 to 0.99984 in the first ship track and to 0.99983 in the second ship track. These results, taken together, demonstrate that the dramatic changes in the internal scattered radiation field within the cloud layer affected by ships arose from increases in the total optical thickness of the cloud layer followed by corresponding decreases in the absorption of solar radiation by a single cloud droplet (as measured by the single scattering albedo). This reduction in the similarity parameter (increase in the single scattering albedo) of the cloud droplets is a direct result of the fact that the droplets are smaller in size in the contaminated portions of the cloud than in the uncontaminated portions (cf. Figure 4). The corresponding reduction in the magnitude of the internal scattered radiation field at 2.20 μm, illustrated in Figure 7, arises from the fact that the total optical thickness of the cloud layer increased, and thus more photons were attenuated at this water absorbing wavelength even though the absorption per drop actually decreased.

Finally, we note that the uncontaminated portion of the cloud layer (at a distance of 63 km) had an optical depth of 11.1 above the aircraft and 9.1 below the aircraft. Had the aircraft been flying at the geometric midlevel of the cloud, one would expect to find 70% of the cloud optical thickness lying above the aircraft with the remainder lying below [*Nakajiima and King*, 1990]. In the first ship track, the bulk of the increase in the total optical thickness of the cloud occurred beneath the aircraft, thus adding support to the view that the source of the particles that contributed to the enhanced concentration and reduced size of the cloud droplets arose from a source beneath the cloud. We believe this source to be particles arising from effluents from ships.

Acknowledgments. The research reported in this article was supported by NASA's Radiation Processes Research Program and the National Science Foundation under grants ATM-8615344 and ATM-8912352. We are grateful to D. P. Wylie of the University of Wisconsin for providing the GOES 6 visible image on July 10, 1987, and to H. G. Meyer and G. T. Arnold for aid in performing the computations and for assistance in data processing. We would further like to acknowledge the coordinating role of the FIRE Science Team, especially D. S. McDougal, D. B. Stroup, and B. A. Albrecht. Finally, we thank *Podzimek* [1989] for directing our attention to *Knott*'s [1923] book on the collected scientific papers of John Aitken, which contains the quotation cited at the beginning of this article.

REFERENCES

Aitken, J., On dust, fogs, and clouds, *Trans. R. Soc. Edinburgh, 30*, 337–368, 1880.

Albrecht, B. A., Aerosols, cloud microphysics, and fractional cloudiness, *Science, 245*, 1227–1230, 1989.

Albrecht, B. A., D. A. Randall, and S. Nicholls, Observations of marine stratocumulus clouds during FIRE, *Bull. Am. Meteorol. Soc., 69*, 618–626, 1988.

Ayers, G. P., J. P. Ivey, and R. W. Gillett, Coherence between seasonal cycles of dimethyl sulphide, methanesulphonate and sulphate in marine air, *Nature, 349*, 404–406, 1991.

Bigg, E. K., J. L. Gras, and C. Evans, Origin of Aitken particles in remote regions of the Southern Hemisphere, *J. Atmos. Chem., 1*, 203–214, 1984.

Braham, R. R., Jr., Cloud physics of urban weather modification—A preliminary report, *Bull. Am. Meteorol. Soc., 55*, 100–106, 1974.

Coakley, J. A., Jr., R. L. Bernstein, and P. A. Durkee, Effect of ship-track effluents on cloud reflectivity, *Science, 237*, 1020–1022, 1987.

Conover, J. H., Anomalous cloud lines, *J. Atmos. Sci., 23*, 778–785, 1966.

Durkee, P. A., Global analysis of aerosol-cloud interaction: Implications for climate change processes, in *Proceedings of the 5th Conference on Satellite Meteorology and Oceanography*, pp. 35–37, American Meteorological Society, Boston, Mass., 1990.

Hansen, J. E., and L. D. Travis, Light scattering in planetary atmospheres, *Space Sci. Rev., 16*, 527–610, 1974.

Hegg, D. A., L. F. Radke, and P. V. Hobbs, Measurements of Aitken nuclei and cloud condensation nuclei in the marine atmosphere and their relation to the DMS-cloud-climate hypothesis, *J. Geophys. Res., 96*, 18,727–18,733, 1991.

Hobbs, P. V., L. F. Radke, and S. E. Shumway, Cloud condensation nuclei from industrial sources and their apparent influence on precipitation in Washington state, *J. Atmos. Sci., 27*, 81–89, 1970.

Hudson, J. G., Effects of CCN concentrations on stratus clouds, *J. Atmos. Sci., 40*, 480–486, 1983.

King, M. D., A method for determining the single scattering albedo of clouds through observation of the internal scattered radiation field, *J. Atmos. Sci., 38*, 2031–2044, 1981.

King, M. D., L. F. Radke, and P. V. Hobbs, Determination of the spectral absorption of solar radiation by marine stratocumulus clouds from airborne measurements within clouds, *J. Atmos. Sci., 47*, 894–907, 1990.

King, M. D., M. G. Strange, P. Leone, and L. R. Blaine, Multiwavelength scanning radiometer for airborne measurements of scattered radiation within clouds, *J. Atmos. Oceanic Technol., 3*, 513–522, 1986.

Knollenberg, R. G., Techniques for probing cloud microstructure, in *Clouds: Their Formation, Optical Properties, and Effects*, edited by P. V. Hobbs and A. Deepak, pp. 15–91, Academic, San Diego, Calif., 1981.

Knott, C. G., *Collected Scientific Papers of John Aitken, LL.D., F.R.S.*, 591 pp., Cambridge University Press, New York, 1923.

Nakajima, T., and M. D. King, Determination of the optical thickness and effective particle radius of clouds from reflected solar radiation measurements. Part I: Theory, *J. Atmos. Sci., 47*, 1878–1893, 1990.

Nussenzveig, H. M., and W. J. Wiscombe, Efficiency factors in Mie scattering, *Phys. Rev. Lett., 45*, 1490–1494, 1980.

Podzimek, J., John Aitken's contribution to atmospheric and aerosol sciences—One hundred years of condensation nuclei counting, *Bull. Am. Meteorol. Soc., 70*, 1538–1545, 1989.

Radke, L. F., Airborne observations of cloud microphysics modified by anthropogenic forcing, in *Proceedings Symposium on the Role of Clouds in Atmospheric Chemistry and Global Climate*, pp. 310–315, American Meteorological Society, Boston, Mass., 1989.

Radke, L. F., and P. V. Hobbs, Cloud condensation nuclei on the Atlantic seaboard of the United States, *Science, 193*, 999–1002, 1976.

Radke, L. F., J. A. Coakley, Jr., and M. D. King, Direct and remote sensing observations of the effects of ships on clouds, *Science, 246*, 1146–1149, 1989.

Scorer, R. S., Ship trails, *Atmos. Environ., 21*, 1417–1425, 1987.

Squires, P., An estimate of the anthropogenic production of cloud nuclei, *J. Rech. Atmos., 2*, 297–308, 1966.

Twomey, S., The nuclei of natural cloud formation, Part II, The supersaturation in natural clouds and the variation of cloud droplet concentration, *Geofis. Pura Appl., 43*, 243–249, 1959.

Twomey, S., Cloud nucleation in the atmosphere and the influence of nucleus concentration levels in atmospheric physics, *J. Phys. Chem., 84*, 1459–1463, 1980.

Twomey, S., and C. F. Bohren, Simple approximations for calcu-

lations of absorption in clouds, *J. Atmos. Sci.*, *37*, 2086–2094, 1980.
Twomey, S., and J. Warner, Comparison of measurements of cloud droplets and cloud nuclei, *J. Atmos. Sci.*, *24*, 702–703, 1967.
Twomey, S., M. Piepgrass, and T. L. Wolfe, An assessment of the impact of pollution on global cloud albedo, *Tellus*, *36*, 356–366, 1984.
van de Hulst, H. C., *Multiple Light Scattering. Tables, Formulas, and Applications*, vols. 1 and 2, 739 pp., Academic, San Diego, Calif., 1980.
Warner, J., and S. Twomey, The production of cloud nuclei by cane fires and the effect on cloud droplet concentration, *J. Atmos. Sci.*, *24*, 704–706, 1967.
Wigley, T. M. L., Possible climate change due to SO_2-derived cloud condensation nuclei, *Nature*, *339*, 355–357, 1989.

P. V. Hobbs, Department of Atmospheric Sciences, University of Washington, Seattle, WA 98195.
M. D. King, NASA Goddard Space Flight Center, Code 900, Greenbelt, MD 20771.
L. F. Radke, Research Aviation Facility, National Center for Atmospheric Research, Boulder, CO 80307.

(Received December 20, 1991;
revised August 27, 1992;
accepted September 2, 1992.)